Journal of Chromatography A 1653 (2021) 462412

Contents lists available at ScienceDirect

Journal of Chromatography A

journal homepage: www.elsevier.com/locate/chroma

Patterns of protein adsorption in ion-exchange particles and columns: Evolution of protein concentration profiles during load, hold, and wash steps predicted for pore and solid diffusion mechanisms

Jürgen Beck[a], Eric von Lieres[b], Negar Zaghi[c], Samuel Leweke[b,e], Giorgio Carta[d], Rainer Hahn[a,*]

[a] Department of Biotechnology, BOKU Vienna, Vienna, Austria
[b] Forschungszentrum Jülich, IBG-1: Biotechnology, 52425 Jülich, Germany
[c] Department of Chemical & Biological Engineering, University of British Columbia, Vancouver, Canada
[d] Department of Chemical Engineering, University of Virginia, Charlottesville, VA, USA
[e] Applied Mathematics, Engineering and Technology, Bayer AG, Leverkusen, Germany

ARTICLE INFO

Article history:
Received 20 May 2021
Revised 6 July 2021
Accepted 7 July 2021
Available online 14 July 2021

Keywords:
Pore diffusion
Solid diffusion
Confocal laser scanning microscopy
Mechanistic modelling
Ion exchange chromatography

ABSTRACT

Elucidation of protein transport mechanism in ion exchanges is essential to model separation performance. In this work we simulate intraparticle adsorption profiles during batch adsorption assuming typical process conditions for pore, solid and parallel diffusion. Artificial confocal laser scanning microscopy images are created to identify apparent differences between the different transport mechanisms. Typical sharp fronts for pore diffusion are characteristic for Langmuir equilibrium constants of $K_L \geq 1$. Only at $K_L = 0.1$ and lower, the profiles are smooth and practically indistinguishable from a solid diffusion mechanism. During hold and wash steps, at which the interstitial buffer is removed or exchanged, continuation of diffusion of protein molecules is significant for solid diffusion due to the adsorbed phase concentration driving force. For pore diffusion, protein mobility is considerable at low and moderate binding strength. Only when pore diffusion if completely dominant, and the binding strength is very high, protein mobility is low enough to restrict diffusion out of the particles. Simulation of column operation reveals substantial protein loss when operating conditions are not adjusted appropriately.

1. Introduction

Ion-exchange chromatography (IEX) is frequently applied for purification of proteins [1]. In comparison to other chromatography modes, e.g., affinity chromatography or hydrophobic interaction chromatography, a very wide range of IEX resins is commercially available, differing in ligand type, physical structure, pore size, and particle size [2–7]. As a result, IEX resins can be used for multiple tasks in downstream processing including protein capture, intermediate purification, and polishing steps, as well as for analytical characterization. With regards to physical structure, IEX resins are typically classified in two categories, macroporous and composite matrices [8,9]. The first type comprises relatively large open pores that provide access to the surface-bound ligands. The liquid phase fills these pores providing the path for protein transport by Fickian diffusion. Typical base matrices in this category are crosslinked agarose, synthetic polymers, and inorganic solids such as silica or hydroxyapatite. Composite media have been introduced to improve binding capacity while preserving mechanical strength and can be further classified into two sub-classes: (1) gel-in-a-shell media, in which a soft, functionalized hydrogel fills the pores of a rigid support matrix; (2) polymer grafted media, where flexible functionalized polymers are linked to the pore surface of a support matrix by either multi-point attachment or single-point attachment [8,10,11].

In general, pore diffusion is the dominant mass transfer mechanism in macroporous media [12,13]. In this case, diffusion of protein molecules occurs in the fluid phase that fills the pore space. If the binding strength is reasonably low, protein molecules can attach to and detach from the ligand many times during transport towards the center of the particle. In contrast, if the binding strength is very high, i.e., when the isotherm is highly favorable or essentially irreversible, individual protein molecules remain at-

* Corresponding author.
E-mail address: rainer.hahn@boku.ac.at (R. Hahn).

https://doi.org/10.1016/j.chroma.2021.462412

tached to the ligand and without further movement. For composite media, the situation is often different. In this case, mass transfer can be partly or completely based on a solid diffusion mechanism where transport occurs in an adsorbed state. This can occur in cases where, because of the flexibility of the hydrogel or polymer grafts, the protein molecules retain diffusional mobility while interacting with the functional ligands. The terms solid diffusion and gel diffusion have also been used to describe this mechanism. Surface diffusion, used to denote transport along a surface, while different on a molecular level, is functionally equivalent since it requires mobility in the surface-bound state. If both pore and adsorbed phase diffusion mechanisms occur simultaneously, the term parallel diffusion is frequently used [14–16]. The two mechanisms result in a very different dependence of the adsorption kinetics on protein concentration and binding strength. For pore diffusion, mass transfer is proportional to the protein fluid phase concentration. Thus, higher rates are always seen at higher solution concentrations. On the other hand, for adsorbed-phase or solid diffusion, mass transfer is related to the bound protein concentration. As a result, the rate is influenced by the shape of the adsorption isotherm. In this case, when the isotherm is highly favorable, the mass transfer rate becomes independent of the protein solution concentration [17].

The dominance of one or the other transport mechanism is determined by the physical structure of the particle. In composite media of type (1) there is hardly any free pore space available and solid diffusion is the sole transport mechanism while in media of type (2), where the pores are not completely occupied by the grafted polymers both mechanisms can contribute to transport. The relative importance of these mechanism is a function of protein solution concentration, adsorption capacity, and of the relative magnitude of the corresponding diffusivities. In general, solid diffusion coefficients are much smaller compared to effective pore diffusivities commonly encountered for practical material [18,19]. However, since the driving force for solid diffusion is proportional to the concentration gradient in the adsorbed phase, this mechanism can still be dominant when the protein solution concentration is low, the binding capacity is high, and the isotherm is highly favorable. In this case, the larger driving force for solid diffusion can more than compensate for the smaller solid phase diffusivity resulting in faster transport than pore diffusion alone [15].

Considering all the above-mentioned aspects, the underlying transport mechanism of a specific protein may be rather complex, especially for multi-component mixtures where hindered diffusion caused by steric hindrance of large bound molecules or, in other cases, coupling of diffusion fluxes can further complicate the adsorption kinetics [20–24]. Elucidating and quantifying protein transport mechanisms is thus important and is needed for the development of accurate mechanistic models that can help accelerate process development for a given separation task.

From a practical viewpoint, elucidation of the mechanism is achieved based on experimental measurements, which can be macroscopic or microscopic. Macroscopic techniques, such as the measurement of the batch adsorption kinetics or the measurement of the response of a chromatographic column to pulse or step changes in protein concentration, rely on comparing experimental results with predictions of models based on different assumption about the underlying mechanism [13]. To be meaningful, such measurements need to cover a range of conditions, such as protein concentration and binding strength, since model discrimination based on measurements at a single condition is extremely limited. In contrast, microscopic techniques that rely on measurements of the patterns of adsorbed protein within an individual particle during transient adsorption provide an improved ability to discriminate among mechanisms. For example, when the isotherm is highly favorable, pore diffusion is expected to result in sharp adsorption fronts, while solid diffusion is expected to result in smooth profiles. Because of these dramatic differences, distinguishing between mechanisms is much easier [25]

Confocal laser scanning microscopy (CLSM) has become very popular for these type of microscopic measurements since its introduction by Ljunglöf and Hjort in 1996 [26]. In this method, a fluorescently labeled protein is used as a marker to determine the bound protein concentration profiles within an individual particle during transient adsorption by taking optical sections of the particle. Since the technique is non-destructive, measurements can be conducted in near real-time. Moreover, using multiple non-interference fluorophores, measurements can be conducted for multicomponent systems. While very powerful, CLSM is also affected by a number of experimental difficulties including artefacts associated with differences between the binding properties of the fluorescent marker and those of the native protein, fluorescence attenuation and light scattering effects, and the opacity of many chromatography particles that require use of refractive index matching fluids [27–31]. Another source of uncertainty, not as commonly appreciated, is the effect of protein mobility within the particles that can potentially affect the results when CLSM is conducted in a batch mode. In this case, if binding is weak or solid diffusion is dominant, significant changes in the bound protein concentration profiles could occur during the measurement itself, potentially skewing the experimental results.

In addition to the effects on microscopic experimental measurements, the nature of the transport mechanism can also potentially affect process performance. The effects of the mass transfer mechanism on column breakthrough and elution behaviors are well understood [12]. In contrast, less is known about the effects on wash and hold steps, which are often components of typical process cycles. During wash steps, used to remove unbound or weakly bound impurities, the protein concentration is zero in the mobile phase fed to the column while the adsorption strength is either unchanged or only slightly weakened compared to that used in the load step. A hold step, during which the protein remains bound without mobile phase flow, can also be included intentionally or between transitions between one step and another. An important question is what happens to the bound protein during these steps. Practically, this is potentially particularly important in multicolumn periodic counter-current systems [32–35]. In such systems, the column being washed is nearly completely saturated which leaves almost no capacity to recapture, downstream, protein molecules that may leave the particles near the column entrance. The extent to which this occurs will determine whether recycling of protein collected in the wash step will be needed or not. Thus, determining the fate of the bound protein molecules during this step is critical.

This work focuses on the simulation of intraparticle profiles that evolve during protein uptake assuming typical process conditions in terms of binding strength and diffusivities. We have created a broad range of artificial CLSM images to identify situations where differences between solid and pore diffusion mechanism are particularly apparent as well as situations at which differentiation becomes increasingly difficult or almost impossible. We have also investigated hold and wash steps by simulated profiles on a particle as well as column level. In this aspect, continuation of diffusion of protein molecules into the particle center but also diffusion from the pore space into the bulk solution plays an essential role and thus can have severe effects on the overall process performance.

There is extensive literature on the mass transfer mechanisms that control the breakthrough behavior of proteins in ion exchange columns, as reviewed, for example, in refs. [12,36]. Less is known, however, about hold and wash behaviors. In this case, while the transport mechanisms can be expected to be the same as those controlling loading, their effects on the evolution of the patterns

of protein bound within the particle and column profiles have not been investigated in detail.

2. Theory and simulation

2.1. Chromatography model

Investigation of adsorption patterns in porous media requires a model describing mass transfer rates. A general model for transport of a solute in spherical beads is given by:

$$\frac{\partial c_p}{\partial t} + \frac{1-\varepsilon_p}{\varepsilon_p}\cdot\frac{\partial q}{\partial t} = D_p\cdot\left(\frac{\partial^2 c_p}{\partial r^2}+\frac{1}{r}\frac{\partial c_p}{\partial r}\right)+\frac{1-\varepsilon_p}{\varepsilon_p}\cdot D_s\cdot\left(\frac{\partial^2 q}{\partial r^2}+\frac{1}{r}\frac{\partial q}{\partial r}\right) \quad (1a)$$

with boundary conditions:

$$D_p\cdot\frac{\partial c_p}{\partial r}(r=0)+\frac{1-\varepsilon_p}{\varepsilon_p}\cdot D_s\cdot\frac{\partial q}{\partial r}(r=0)=0 \quad (1b)$$

$$D_p\cdot\frac{\partial c_p}{\partial r}(r=r_p)+\frac{1-\varepsilon_p}{\varepsilon_p}\cdot D_s\cdot\frac{\partial q}{\partial r}(r=r_p)=\frac{k_f}{\varepsilon_p}\cdot\frac{3}{r_p}\cdot(c-c_p) \quad (1c)$$

where c_p is the solute concentration in the intraparticle fluid phase, q the adsorbed concentration, ε_p the intraparticle porosity, r_p the radius of the particle, D_s and D_p the solid and pore diffusion coefficient and k_f the film mass transfer coefficient.

Eq. (1) describes a general model of parallel transport which reduces to the pore diffusion model and solid diffusion model, by setting the corresponding diffusion coefficients D_s or D_p to zero. To describe a batch process, Eq. (1) is coupled with the material balance:

$$\frac{\partial c}{\partial t}=-\frac{1-\varepsilon_b}{\varepsilon_b}\cdot k_f\cdot\frac{3}{r_p}\cdot(c-c_p(r=r_p)) \quad (2a)$$

$$c_p(t=0)=q(t=0)=0 \quad (2b)$$

$$c(t=0)=c_F \quad (2c)$$

In Eq. (2), the term $\varepsilon_b = V_b/V$ denotes the batch porosity, V total batch volume and V_b liquid batch volume, i.e., without solid and pore volumes of particles. Consequently, $(1-\varepsilon_b)/\varepsilon_b = (V-V_b)/V_b$ with the volume occupied by particles defined as $V_p = V-V_b$. Mass transfer into the particles is determined by the film mass transfer coefficient k_f, which can be estimated through engineering correlations. c_F is the concentration of the protein solution with c being the concentration in the bulk fluid. The same symbol will be used for the concentration of the protein solution for column adsorption.

To describe a column operation, the following equation and boundary conditions replace Eq. (2) with:

$$\frac{\partial c}{\partial t}=-\nu\cdot\frac{\partial c}{\partial z}+D_{ax}\cdot\frac{\partial^2 c}{\partial z^2}-\frac{1-\varepsilon_c}{\varepsilon_c}\cdot k_f\cdot\frac{3}{r_p}\cdot(c-c_p(r=r_p)) \quad (3a)$$

Boundary conditions

$$c(t=0)=c_0 \quad (3b)$$

$$\nu c(z=0)-D_{ax}\cdot\frac{\partial c}{\partial z}(z=0)=\nu\cdot c_{Feed} \quad (3b)$$

$$\frac{\partial c}{\partial z}(z=L)=0 \quad (3d)$$

Here, $\varepsilon_c = V_c/V$ denotes column porosity, V total column volume and V_c interstitial (or extraparticle) column volume, hence the particle volume is $V_p = V\text{-}V_C$. D_{ax} is the axial dispersion coefficient and ν is the interstitial velocity. Initial and boundary conditions are specified with c_0 being the initial concentration, which is equal to 0 for loading a clean column and c_{Feed} as the protein concentration in the liquid supplied to the column, which is equal to c_F for loading and to 0 for hold and wash steps. For the numerical simulations reported in this work, we assumed sufficiently fast binding kinetics to achieve local equilibrium between the local protein concentration in the particle pores c_p, and the local bound protein concentration q, according to the Langmuir adsorption isotherm:

$$q=q_{max}\frac{K_L\cdot c_p}{1+K_L\cdot c_p} \quad (4)$$

It should be noted that while the Langmuir isotherm does not have an explicit dependence on ionic strength, the value of K_L is expected to decrease as a function of salt concentration as a result of the weakened electrostatic interaction. A description of this effect can be obtained, for example, using the steric mass action (SMA) law model [37] which accounts explicitly for the effect of salt concentration. In practice, however, the Langmuir isotherm with parameters regressed at each salt concentration and the SMA model with parameters globally fitted to data over a range of salt concentrations provide comparable descriptions of typical data. For example, for the lysozyme/S-HyperD system in 10 mM sodium phosphate at pH 6.5 studied by Lewus and Carta (1999) [38], K_L ~ 100 without addition of NaCl, while K_L ~ 0.65 with the addition of 150 mM NaCl. Thus, the values of K_L used in this work in the range 0.1-1000 are realistic and bracket values observed experimentally.

Throughout the work we used following conditions: $c_F = 2.0$g/L, maximum binding capacity of the resin $q_{max} = 750$ g/L solid phase which equals 150 g/L particle, particle radius $r_p = 37.5$ µm and intraparticle porosity $\varepsilon_p = 0.8$. The Langmuir equilibrium constant K_L was varied to define different binding strengths.

2.2. Batch adsorption

Batch adsorption was simulated as a shallow bed operated at a flow rate sufficiently high to prevent significant change of the bulk fluid concentration. For our simulations we used a 1 mL column that was loaded and washed at a flow rate of >10 mL/min. Intraparticle protein concentration over time was calculated with the given adsorption parameters and the macroscopic uptake curve was constructed from the mass balance.

2.3. Hold and wash steps

Hold and wash step simulations were modelled for two cases. In the first case, a "hydrated particle" model was set-up to study transport within the particle without external liquid. For this purpose, a minimal amount of extra-particle space was adjusted, $\varepsilon_b = 0.0001$ in Eq. (2), which translates to the volume of particles being roughly equal to the total volume $V_p \sim= V$. The resin was loaded for 120 s (20-50% saturation depending on type of diffusion) at 10 mL/min to ensure sufficient saturation. Subsequently, the column was washed for 10 s until no protein remained in the bulk fluid. Then, a hold step was implemented by lowering the flow rate to almost zero (~ 0.0001 mL/min). For the second case, a wash step after adsorption was simulated by exposing a small amount of resin to a large buffer excess, representing an infinite bath. In this case, the model was created by using a large extra-particle space $\varepsilon_b = 0.9999$ or $V_p << V$. Simulations were performed for pore, solid and parallel diffusion cases at selected binding strengths.

2.4. Column adsorption

A 10 mL (i.d. = 1 cm, L = 12.7 cm) column was operated at a residence time of 3 min, with axial dispersion $D_{ax} = 5.25\cdot10^{-4}$

cm^2/s, and $k_f = 2.0 \cdot 10^{-3}$ cm/s based on correlations described in [39–41]. The column was loaded to 10 % and 80 % dynamic breakthrough, respectively, with different mass transport mechanisms and binding strengths. Then a wash step was applied for 10 column volumes (CV). The concentration profile was evaluated and loss during wash out was quantified by integration with the trapezoidal method.

2.5. Software

The Chromatography Analysis and Design Toolkit (CADET) Version 4.1.0 was used for all chromatographic simulations in this paper (https://cadet.github.io) [42]. The one-dimensional general rate model available in CADET was used to generate both intraparticle and column profiles using selected values of the diffusivities and Langmuir equilibrium constants. The calculated radial intraparticle concentration profiles were then exported and used to construct a colormesh in a polar coordinate system with intensity proportional to the bound concentration value using Python's matplotlib package. Python 3.6 was used for creating the simulated CLSM images and for data processing. The numerical solutions were verified with analytical solutions (if available) and independent calculations based on numerical methods described in [43].

3. Results

3.1. Intraparticle profiles during batch uptake

For the initial examination of macroscopic uptake and comparison of intraparticle profiles during adsorption a shallow bed model was set up. We selected particle diffusion coefficients, particle properties and adsorption capacities which are representative for typical protein purification tasks [13].

Two different cases were considered for the simulations. In the first of these, we consider the behavior of an adsorbent particle where transport is dominated by solid diffusion; i.e., with $D_p = 0$. A practical example is the case of lysozyme on S-Hyper D described in ref. [17] which is a composite resin consisting of a silica matrix whose pores are essentially completely filled with a charged gel. It has been shown that in this resin lysozyme diffuses and binds throughout the gel with a solid diffusion coefficient $D_s = 7.0 \cdot 10^{-9}$ cm^2/s. In the second case, we consider diffusion and binding into a hypothetical macroporous resin where transport is dominated by pore diffusion; i.e., with $D_s = 0$. In order to facilitate comparisons with the solid diffusion case, we selected a value of $D_p = 3.5 \cdot 10^{-7}$ cm^2/s, which gives overall adsorption rates close to those observed for solid diffusion with $D_s = 7.0 \cdot 10^{-9}$ cm^2/s. This value of D_p can be connected to an actual physical system by means of established estimation methods. For instance, for lysozyme, which has a free solution diffusivity of about $1 \cdot 10^{-6}$ cm^2/s [44], assuming a pore radius of 20 nm results in a hindrance factor of about 0.7 [24,45]. Accordingly, using a typical tortuosity factor of 2, we obtain $D_p = 1 \cdot 10^{-7}$ x $0.7/2 = 3.5 \cdot 10^{-7}$ cm^2/s, which is the same as that used in our simulations. A similar value of Dp has been obtained experimentally for lysozyme on the resin SP-Sepharose-FF [46]. It should be noted that solid diffusion has also been observed for larger proteins, including IgG [22,47]. Thus, we expect solid diffusion behaviors for larger proteins to be qualitatively similar to those seen for lysozyme. In the case of pore diffusion, the main difference between smaller and larger proteins is expected to be the different degree of diffusional hindrance, which will be dependent on the ratio of protein to pore size. Similar behavior is expected if this ratio is similar.

In Fig. 1A the macroscopic adsorption profiles almost completely overlap. However, at the selected conditions, the intraparticle profiles simulated are substantially different. In a solid diffusion mechanism, protein molecules migrate very fast and reach the core of the particle after ~2 minutes. In contrast, profiles for pore diffusion appear as sharp fronts that travel to the center of the particle over time. Profiles shown in Fig. 1B are well known and have been used by several researchers to elucidate the dominating mass transfer mechanism based on their typical appearance [25]. One motivation for this work was the question whether there are adsorption conditions where differentiating between mechanisms becomes difficult. Based on adsorption theory, pore diffusion at low binding strength also gives smooth profiles, similar to those observed for solid diffusion. In fact, if the isotherm is linear, the profiles predicted for pore and solid diffusion become identical to each other provided that one takes $\varepsilon_p D_p = q_{max} D_s / c_F = q_{max} \cdot K_L \cdot D_s$, where $q_{max} \cdot K_L$ is the initial slope of the isotherm [36]. In such cases the adsorbed protein is not strongly bound but is attached on and detached from the adsorbing surface many times during diffusion to the particle center. Fig. 2 compares the adsorption kinetics and the corresponding adsorbed protein concentration profiles predicted by the pore with $D_p = 1.1 \cdot 10^{-7}$ cm^2/s and an almost linear isotherm at $K_L = 0.1$ with those predicted by the solid diffusion model with $D_s = 7.0 \cdot 10^{-9}$ cm^2/s and $K_L = 100$, all the other conditions having been kept constant.

As seen in this figure, both the overall kinetics (Fig. 2A) and the adsorbed concentration profiles (Fig. 2B) are nearly coincident. Obviously, for these conditions it would not be possible to discriminate between transport mechanism without an independent knowledge of the isotherm.

To bridge the gap between conceptional dimensionless radial profiles and intuitive (empirical) understanding of transport mechanism by visual inspection, simulated CLSM images were created based on numerically predicted intraparticle profiles for different conditions. Fig. 3 shows these profiles (Fig. 3A) and corresponding simulated CLSM images for pore diffusion with $D_p = 1.1 \cdot 10^{-7}$ cm^2/s and different K_L values as well as solid diffusion with $D_s = 7.0 \cdot 10^{-9}$ cm^2/s with $K_L = 100$. We have included a figure showing the relevant isotherm profiles in the supplementary materials (Fig. S1). Consistent with the experimental practice of confocal microscopy, where, to ensure the proper dynamic range, the laser intensity is chosen based on the fluorescence of a saturated particle. The simulated CLSM profiles are normalized to the respective maximum value of q, which is observed at the particle surface. As can be seen in Fig. 3B, a low binding strength of $K_L = 0.1$ results in a smooth profile while values of $K_L > 1$ result in the typical sharp adsorption fronts normally associated with pore diffusion. As noted, before, solid diffusion with $K_L = 100$ and pore diffusion with $K_L = 0.1$ have identical appearance.

With this tool in hand, we turn our attention to the general aspect of protein mobility in the adsorbed phase for three different cases. In the first we consider particles initially loaded with protein to achieve partial separation followed by removal of the external liquid phase. In the second we consider a "zero length" column where particles partially saturated with protein are suddenly exposed to a solution containing no protein at a high flow rate. Finally, we consider the wash step of a finite length column partially saturated with protein with a finite flow rate of the mobile phase.

3.2. Batch adsorption with hold step

Fig. 4 shows simulated CLSM images for particles that are loaded with protein for 120 seconds, which results in loadings of 20-50 % of q_{max}, followed by a simulated hold where the external protein concentration is suddenly dropped to zero while no protein can diffuse out of the particles. The same value of K_L was used during load and wash and results are shown for different values of K_L.

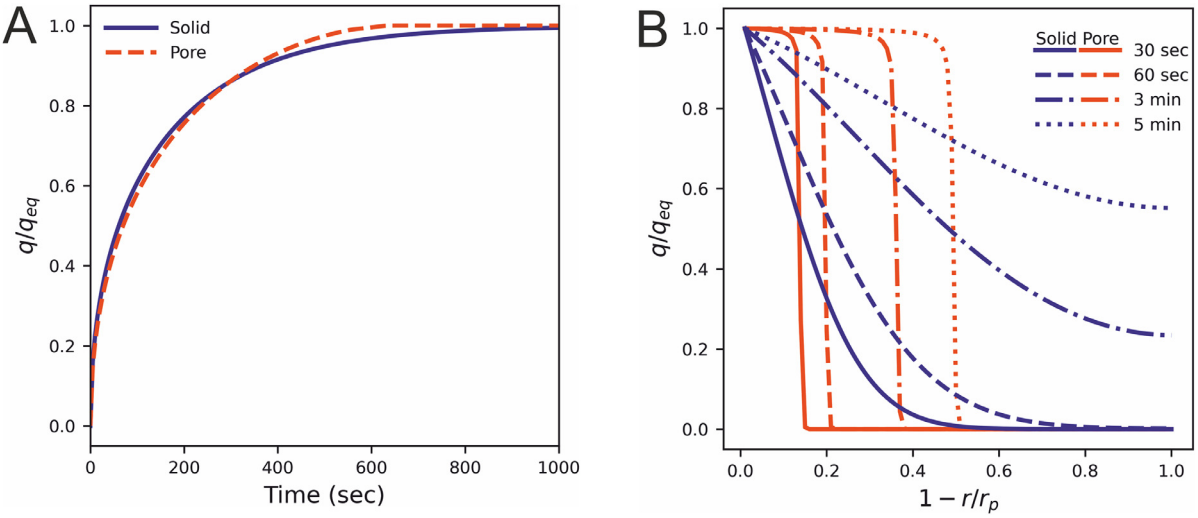

Fig. 1. Macroscopic uptake curves (A) and intraparticle profiles (B) with dimensionless binding capacity (q normalized by the respective equilibrium capacity q_{eq}) over time in a shallow bed. Adsorption was simulated with $c_F = 2.0$ mg/mL and $qmax = 150$ mg/mL for pure solid diffusion $K_L = 100$ mL/mg, $D_s = 7.0{\cdot}10^{-9}$ cm^2/s (blue) and rectangular isotherm pore diffusion (shrinking core) $K_L = 100$ mL/mg, $D_p = 3.5{\cdot}10^{-7}$ cm^2/s (orange).

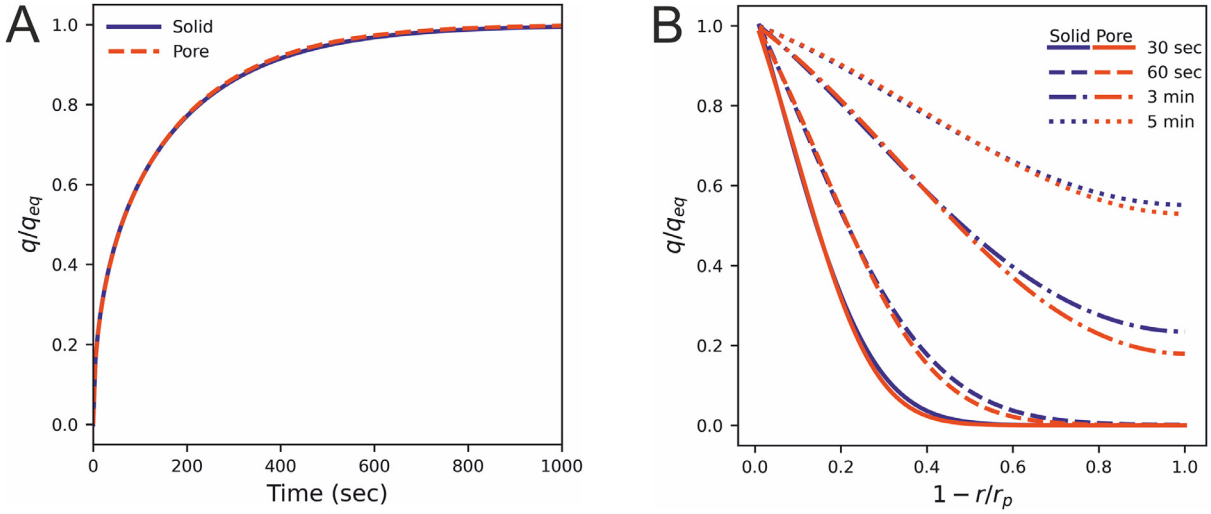

Fig. 2. Macroscopic uptake curves (A) and intraparticle profiles (B) over time in a shallow bed. Adsorption was simulated with $c_F = 2.0$ mg/mL and $q_{max} = 150$ mg/mL for pure solid diffusion $K_L = 100$ mL/mg, $D_s = 7.0{\cdot}10^{-9}$ cm^2/s (blue) and rectangular isotherm pore diffusion (shrinking core) $K_L = 0.1$ mL/mg, $D_p = 1.1{\cdot}10^{-7}$ cm^2/s (orange).

In practice, these conditions correspond to those used in a batch CLSM experiment where the particles are separated from the protein solution by suction through a frit, centrifugation, or filtration [48]. For solid diffusion, the driving force is the gradient in adsorbed phase concentration. As seen in Fig. 4, the pore diffusion model predicts almost no change in the bound protein profile during the hold period except when K_L is very small (<1). When K_L is low, the protein detaches from the surface and is redistributed across the particle radius. For higher values of K_L, this redistribution is absent, and the protein molecules are virtually immobilized on the surface. A different result is obtained from the solid diffusion model. In this case, even if K_L is large (e.g., 100), since the adsorbed protein remains mobile, even after just a 60 s hold, the adsorbed protein concentration profile changes substantially. After 10 min, the protein is almost completely redistributed resulting in a nearly homogenous distribution across the particle radius.

Recent advances in protein chromatography, in particular ion-exchange chromatography, was triggered by the introduction of composite and grafted chromatography materials [8,9]. On one hand, adsorption capacities were remarkably increased, and on the other hand, mass transfer was also substantially enhanced. These improvements were widely investigated and reported by several authors. Accelerated mass transport was commonly attributed to a parallel diffusion mechanism in which a certain contribution of solid phase transport occurs in the polymeric network in addition to pore diffusion [49–52]. Mass transport of proteins solely based on solid diffusion seems to be restricted to gel-in-a-shell media. Moreover, it has been previously demonstrated that weak binding conditions in buffers with higher conductivity can cause similar effects in conventional macroporous media [53]. As a likely scenario we have simulated adsorption for solid, pore and parallel diffusion at $K_L = 10$ (Fig. 5).

The patterns after 3- and 10-minutes hold time appear very characteristic for the respective mass transfer type. Obviously, discrimination between solid and parallel diffusion is not straightforward but the fact that solid diffusion contributes significantly to overall mass transfer can be concluded from a single measurement. Additional examples of parallel transport behavior are shown in the supplementary materials (Figures S2 to S4). Our simulations reveal that for solid and pore diffusion at low K_L, the diffusional

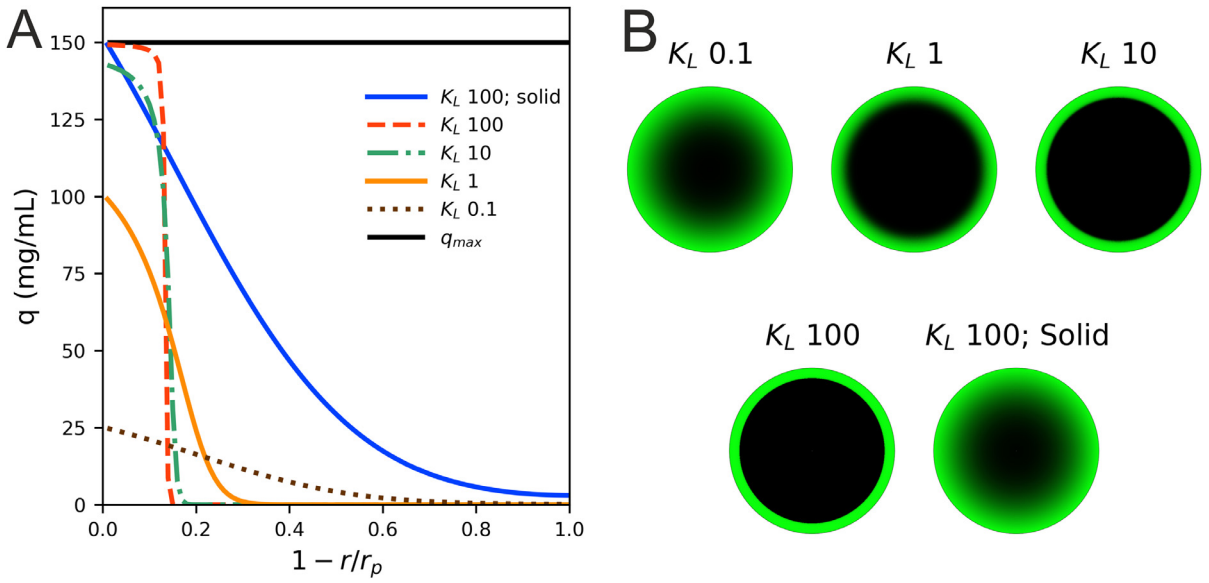

Fig. 3. A) Adsorption fronts after 90 seconds of loading for different binding strengths of pore diffusion with $D_p = 1.1 \cdot 10^{-7}$ cm^2/s and solid diffusion with $D_s = 7.0 \cdot 10^{-9}$ cm^2/s; B) Corresponding simulated CLSM images normalized to equilibrium capacity.

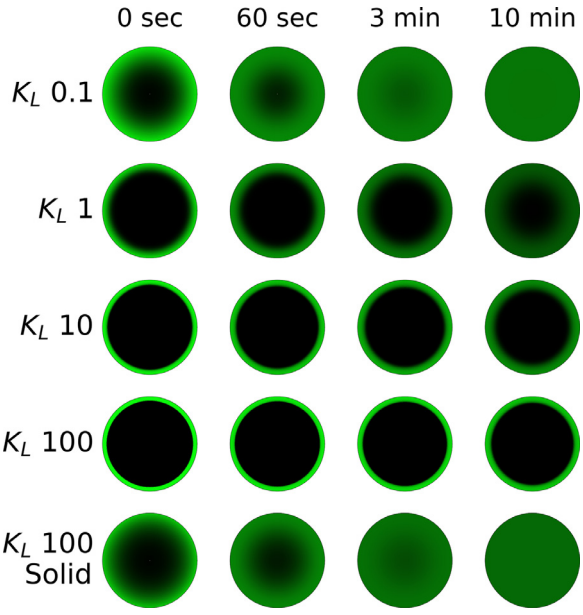

Fig. 4. Simulated CLSM images of a hold step in hydrated resin; progression of adsorption front from end of load (120 seconds) to 10 minutes for pore diffusion at different binding strengths with $D_p = 1.1 \cdot 10^{-7}$ cm^2/s and solid diffusion $D_s = 7.0 \cdot 10^{-9}$ cm^2/s.

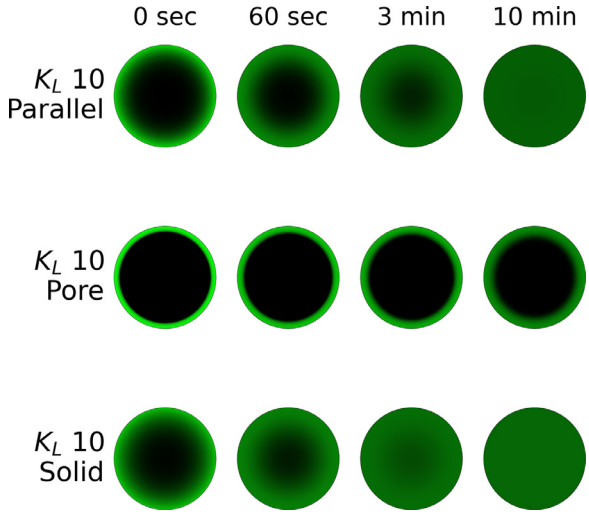

Fig. 5. Simulated CLSM images of a hold step in hydrated resin; progression of adsorption front from end of load (120 seconds) to 10 minutes of pore diffusion with $D_p = 1.1 \cdot 10^{-7}$ cm^2/s, solid diffusion with $D_s = 7 \cdot 10^{-9}$ cm^2/s and parallel diffusion with $D_p = 1.1 \cdot 10^{-7}$ and $D_s = 4.0 \cdot 10^{-9}$ cm^2/s (chosen to match uptake kinetics of solid diffusion case) at medium binding strength in a hydrated particle type simulation.

process into the center of the particle continues unaffectedly even when the external liquid is removed. This behavior has certain implications: At certain conditions there is a possibility of overestimating mass transport on CLSM measurements when the time between the removal of the liquid phase and the actual measurement is too long. The use of a more complicated CLSM flow cell measurement can overcome this problem. Otherwise, one could benefit from the experimental set-up, that was simulated in Fig. 4 and Fig. 5 to simplify mass transport assessment. Loading up to 20-50 % saturation and introducing an intentional hold step before measurement can provide a profile that is characteristic for a specific mass transfer type. A prerequisite is that the binding strength must be known from isotherm or isocratic elution data. This information can be obtained experimentally using a variety of techniques, including batch uptake measurements and isocratic elution conducted at different salt concentrations and gradient elution experiments conducted over a range of gradient slopes as reviewed, for example, in Carta et al., [46].

3.2. Batch adsorption with simulated wash step

Fig. 6 shows the simulated CLSM images (Fig. 6A) and the overall adsorption kinetics (Fig. 6B) during a simulated wash step for the same conditions of Fig. 4. In this case, the volume of liquid surrounding the particle is essentially infinite, which keeps the external concentration at zero, but, unlike the previous case, pro-

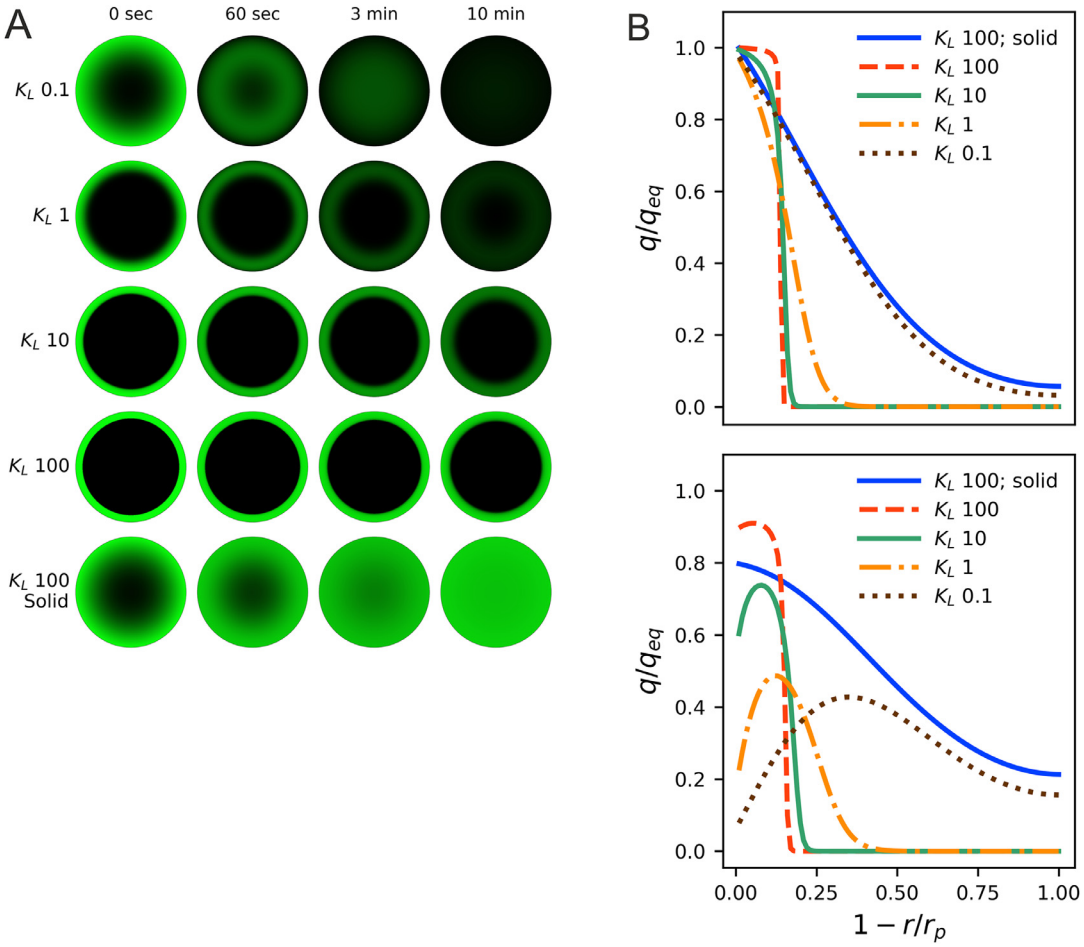

Fig. 6. A) Simulated CLSM images of a hold step in infinite bath initially devoid of protein. Progression of adsorption front from end of load (120 seconds) to 10 minutes for pore diffusion at different binding strengths with $D_p = 1.1 \cdot 10^{-7}$ cm^2/s and solid diffusion $D_s = 7.0 \cdot 10^{-9}$ cm^2/s. B) Intraparticle profiles at the end of the load step (top) and after 60 seconds hold in infinite bath (bottom).

tein molecules bound during the load step can diffuse out of the particle. Different results are predicted again for the two models depending on the value of K_L. For strong binding conditions ($K_L = 100$) the patterns are similar to the situation of a hold step with no external fluid. For solid diffusion, protein molecules continue to diffuse rapidly toward the particle center resulting in a redistribution of bound protein across the particle radius. Note that little protein diffuses out of the particle for these conditions, which results is very favorable partitioning toward the particle at the external particle-fluid interface. Because of this favorable partitioning, the fluid-phase protein concentration remains near zero at the particle surface greatly reducing the rate of external transport. For pore diffusion with $K_L = 100$, the adsorbed protein molecules are immobile and external there is no change even after a long time. Moreover, there is also no loss of protein from the particle, since, because of favorable binding, external transport is again extremely slow. For pore diffusion with lower K_L values the situation is different. In this case, the driving force is the concentration gradient in the fluid phase. If K_L is very low and partitioning is not so favorable, the protein bound during the load step is in part redistributed across the particle radius and in part leaves the particle. For long times and small values of K_L, almost all the initially bound protein is lost. As a result, for these low-K_L conditions, the bound protein concentration profile has a maximum at intermediate times. This maximum disappears for larger K_L values (e.g., $K_L \sim 100$) when little protein is lost from the particle.

3.3. Column adsorption

Clearly, an infinite bath represents an idealized, unrealistic scenario intended to simplify the modelling of adsorption situation. However, results from the simulations shown in Fig. 6, suggest an important impact of the diffusion mechanisms as well the binding strength on wash and hold steps during column operation.

Fig. 7 shows the results obtained for a finite length column partially saturated with a protein followed by an extensive wash step using same diffusion coefficients and varying adsorption strength as for batch adsorption. These results show the column effluent concentration profile with 0 CV corresponding to the start of the wash step. We used two different levels of column saturation, corresponding to a DBC 80% (Fig. 7A) and to a DBC of 10 % (Fig. 7B). The former is comparable to the situation encountered in periodic countercurrent chromatography (PCC) processes whereas the latter is representative of a conventional batch column process [54–56]. Reference to the PCC process is made to highlight a case where the column is nearly fully loaded prior to the wash step. When a single column is used, only partial loading, up to the dynamic binding capacity, is possible in practice. The two cases are exemplified by Fig. 7A and 7B, respectively.

As seen in Fig. 7A, losses of protein in the wash phase are substantially larger for the cases with high saturation regardless of the adsorption strength and the mass transfer mechanism compared to the case with low initial column saturation (Fig. 7B). The fraction that is lost increases with decreasing binding strength (i.e., lower

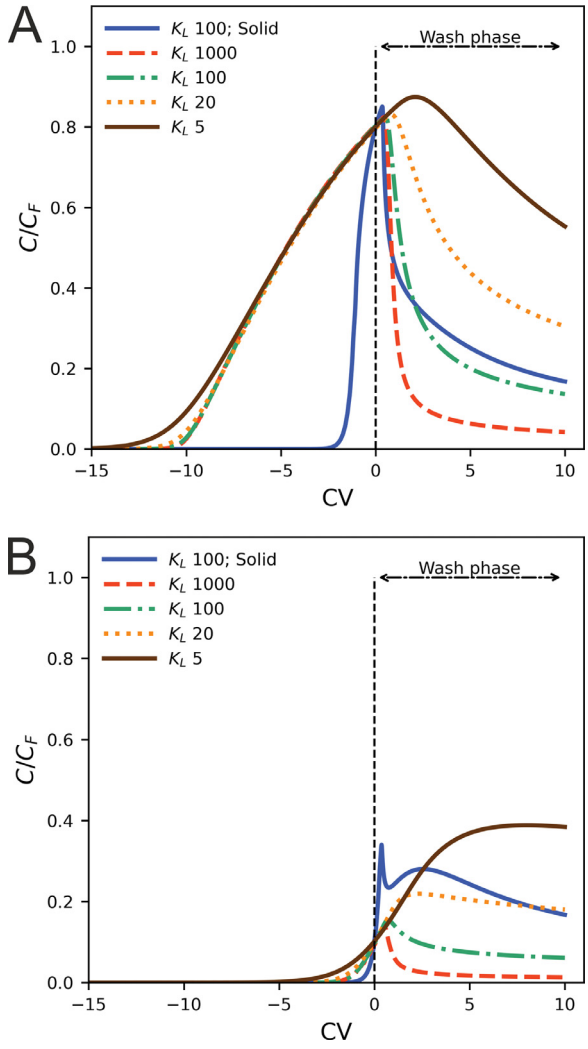

Fig. 7. Simulation of column adsorption process with wash step. Column was loaded at a residence time of 3 min with protein solution (c_F = 2.0 mg/mL, q_{max} = 150 mg/mL) to DBC 80 % (A) and DBC 10 % (B). The column was then washed for 10 CV to investigate the losses during the wash step at different binding strengths for a pore diffusion coefficient $D_p = 1.1 \cdot 10^{-7}$ cm^2/s compared to solid diffusion $D_s = 7.0 \cdot 10^{-9}$ cm^2/s at K_L = 100 mL/mg. The wash step starts at CV=0.

Table 1
Protein loss during the wash step of column loaded with protein to saturation levels of 80 and 10%. Loss is given as percentage of the amount of protein loaded, which is lost during a 10 CV wash for $D_p = 1.1 \cdot 10^{-7}$ cm^2/s and $D_s = 7.0 \cdot 10^{-9}$ cm^2/s.

	K_L (mL/mg)	Loss (%) DBC 80 %	DBC 10 %
Pore	5	15.0	8.5
	20	9.6	4.7
	100	5.4	2.1
	1000	2.6	0.8
Solid	100	6.0	4.8

K_L). However, at K_L = 100 or even K_L = 1000, only a small fraction is washed out. A quantitative analysis of protein losses was performed based on a PCC process where the breakthrough from the first column is typically loaded to the next column. As such only the true wash out starting at CV = 0 was considered for the 80% saturated column. For the lower saturation, the loss due to breakthrough was included though this contribution is small. The resulting protein losses calculated from integration of the profiles and expressed as a percentage of the protein loaded are summarized in Table 1.

It can be observed from Fig. 7 that, for the conditions simulated, mass transfer for solid diffusion is much faster resulting in a very steep breakthrough curve. Due to the different driving force the shape of the wash out curves differed significantly from those for pore diffusion. Since, in the case of solid diffusion, the protein retains diffusional mobility more protein is washed out compared to the case of pore diffusion at equivalent binding strengths. This is especially evident for the low initial saturation case (Fig. 7B). In this case, when K_L is large, the bound protein is essentially immobilized while significant binding capacity is available at the end of the load step to recapture any unbound protein left in the particle pores and in the extraparticle fluid. When K_L is large, most of this protein is adsorbed during the wash step and not lost in the effluent. On the other hand, for solid diffusion, all of the protein loaded is mobile, which results in greater losses and a distinct difference in curve shapes during the wash step. The higher spike in protein concentration observed for solid diffusion at K_L = 100, which is absent in pore diffusion at K_L = 100, is the result of the much sharper breakthrough curve. The extent of saturation needed to achieve a $C/C_F = 0.1$ breakthrough concentration in the solid diffusion case is much greater. Therefore, the protein concentration near the column outlet is higher and the concentration spike is seen in the early stages of the wash step. Following this early concentration spike, more protein continues to be found in the wash for the solid diffusion case, because the bound protein retains diffusional mobility and can leak out of the particle at a greater rate than for pore diffusion at equal binding strength. The losses are obviously greater with a high initial saturation for both mechanisms since, in this case, there is little residual binding capacity to adsorb the protein before it is lost in the effluent. Hence, in such a situation recycling of the wash fraction is required to maintain a high yield and productivity when operating in a PCC system [57]. The influence of the film mass transfer was also studied by simulating adsorption and wash out at different velocities (see Figure S5 in supplementary materials). Film mass transfer coefficients were adjusted based on correlations for column operation. Overall, operating the column at higher velocities minimizes the loss in the wash out fraction to a minor extent. Though film mass transfer coefficients increase at high velocities and favor protein diffusion out of the particles, the much shorter cycle time overcomes this effect leading to reduced protein wash out.

4. Conclusions

Pore and solid diffusion are distinguished by the difference in their driving force. At strong binding conditions the intraparticle profiles are characteristic for the respective mechanisms. Pore diffusion exhibits sharp fronts and solid diffusion smooth transitional profiles. When the binding strength decreases in a pore diffusion system, the profiles gradually approach the solid diffusion pattern. Eventually at very low binding strength K_L = 0.1, the profiles are practically indistinguishable when there is no diffusion to the outside of the particle. Understanding the underlying mechanism of a particular chromatographic separation process is critical. For adsorption, solid diffusion contribution accelerates mass transfer allowing to work a high flow rate. In turn, during wash and hold steps, the continuing transport can lead to substantial protein diffusion out of the particles, especially at high column saturation.

The simulations performed in this work were mostly based on a single diffusion mechanism. This was necessary to identify the most prominent effects on specific operation conditions. In practical work, many resins will exhibit a parallel transport behavior. Furthermore, complex feedstocks result in multi-component ad-

sorption situations which further complicates understanding of the underlying principles. Depending on the dominance of one or the other mass transfer mechanism, which also strongly depends on buffer conditions, our calculations can contribute to better process understanding and design.

Declaration of competing interest

The authors declare that they have no known competing financial interests or personal relationships that could have appeared to influence the work reported in this paper.

CRediT authorship contribution statement

Jürgen Beck: Conceptualization, Investigation, Data curation, Formal analysis, Methodology, Validation, Visualization, Writing – original draft. **Eric von Lieres:** Conceptualization, Funding acquisition, Project administration, Resources, Supervision, Validation, Writing – review & editing. **Negar Zaghi:** Investigation, Data curation. **Samuel Leweke:** Validation, Supervision, Writing – review & editing. **Giorgio Carta:** Validation, Writing – review & editing. **Rainer Hahn:** Conceptualization, Funding acquisition, Project administration, Resources, Supervision, Validation, Writing – review & editing.

Acknowledgements

The authors would like to thank our colleague Dr. Nico Lingg for proofreading and helpful discussions.

Supplementary materials

Supplementary material associated with this article can be found, in the online version, at doi:10.1016/j.chroma.2021.462412.

References

[1] S. Yamamoto, Ion-Exchange Chromatography of Proteins, Routledge CRC Press. (1988).
[2] A. Staby, I.H. Jensen, I. Mollerup, Comparison of chromatographic ion-exchange resins: I. Strong anion-exchange resins, J. Chromatogr. A. 897 (2000) 99–111, doi:10.1016/S0021-9673(00)00780-9.
[3] A. Staby, I.H. Jensen, Comparison of chromatographic ion-exchange resins: II. More strong anion-exchange resins, J. Chromatogr. A. 908 (2001) 149–161, doi:10.1016/S0021-9673(00)00999-7.
[4] A. Staby, M.-B. Sand, R.G. Hansen, J.H. Jacobsen, L.A. Andersen, M. Gerstenberg, U.K. Bruus, I.H. Jensen, Comparison of chromatographic ion-exchange resins: III. Strong cation-exchange resins, J. Chromatogr. A. 1034 (2004) 85–97, doi:10.1016/j.chroma.2004.01.026.
[5] A. Staby, M.-B. Sand, R.G. Hansen, J.H. Jacobsen, L.A. Andersen, M. Gerstenberg, U.K. Bruus, I.H. Jensen, Comparison of chromatographic ion-exchange resins: IV. Strong and weak cation-exchange resins and heparin resins, J. Chromatogr. A. 1069 (2005) 65–77, doi:10.1016/j.chroma.2004.11.094.
[6] A. Staby, J.H. Jacobsen, R.G. Hansen, U.K. Bruus, I.H. Jensen, Comparison of chromatographic ion-exchange resins: V. Strong and weak cation-exchange resins, J. Chromatogr. A. 1118 (2006) 168–179, doi:10.1016/j.chroma.2006.03.116.
[7] A. Staby, R.H. Jensen, M. Bensch, J. Hubbuch, D.L. Dünweber, J. Krarup, J. Nielsen, M. Lund, S. Kidal, T.B. Hansen, I.H. Jensen, Comparison of chromatographic ion-exchange resins: VI. Weak anion-exchange resins, J. Chromatogr. A. 1164 (2007) 82–94, doi:10.1016/j.chroma.2007.06.048.
[8] A.M. Lenhoff, Protein adsorption and transport in polymer-functionalized ion-exchangers, J. Chromatogr. A. 1218 (2011) 8748–8759, doi:10.1016/j.chroma.2011.06.061.
[9] E. Müller, Properties and characterization of high capacity resins for biochromatography, Chem. Eng. Technol. 28 (2005) 1295–1305, doi:10.1002/ceat.200500161.
[10] A. Staby, J. Nielsen, J. Krarup, M. Wiendahl, T. Hansen, S. Kidal, J. Hubbuch, J. Mollerup, Advances in Resins for Ion-Exchange Chromatography, Adv. Chromatogr. 47 (2009) 193–245, doi:10.1201/9781420060379.ch6.
[11] L. Yu, Y. Sun, Recent advances in protein chromatography with polymer-grafted media, J. Chromatogr. A. 1638 (2021) 461865, doi:10.1016/j.chroma.2020.461865.
[12] G. Carta, A. Jungbauer, Protein Chromatography, John Wiley & Sons, Ltd, 2020. https://doi.org/10.1002/9783527824045.
[13] R. Hahn, Methods for characterization of biochromatography media, J. Sep. Sci. 35 (2012) 3001–3032, doi:10.1002/jssc.201200770.
[14] H. Yoshida, M. Yoshikawa, T. Kataoka, Parallel transport of BSA by surface and pore diffusion in strongly basic chitosan, AIChE J 40 (1994) 2034–2044, doi:10.1002/aic.690401213.
[15] A.K. Hunter, G. Carta, Protein adsorption on novel acrylamido-based polymeric ion exchangers: II. Adsorption rates and column behavior, J. Chromatogr. A. 897 (2000) 81–97, doi:10.1016/S0021-9673(00)00865-7.
[16] W.-D. Chen, X.-Y. Dong, Y. Sun, Analysis of diffusion models for protein adsorption to porous anion-exchange adsorbent, J. Chromatogr. A. 962 (2002) 29–40, doi:10.1016/S0021-9673(02)00466-1.
[17] R.K. Lewus, F.H. Altan, G. Carta, Protein adsorption and desorption on gel-filled rigid particles for ion exchange, Ind. Eng. Chem. Res. 37 (1998) 1079–1087, doi:10.1021/ie970506z.
[18] M.A. Fernandez, W.S. Laughinghouse, G. Carta, Characterization of protein adsorption by composite silica-polyacrylamide gel anion exchangers II. Mass transfer in packed columns and predictability of breakthrough behavior, J. Chromatogr. A. 746 (1996) 185–198, doi:10.1016/0021-9673(96)00338-X.
[19] L.E. Weaver, G. Carta, Protein adsorption on cation exchangers: comparison of macroporous and gel-composite media, Biotechnol. Prog. 12 (1996) 342–355, doi:10.1021/bp960021q.
[20] Y. Tao, G. Carta, G. Ferreira, D. Robbins, Adsorption of deamidated antibody variants on macroporous and dextran-grafted cation exchangers: II. Adsorption kinetics, J. Chromatogr. A. 1218 (2011) 1530–1537, doi:10.1016/j.chroma.2011.01.050.
[21] Y. Tao, E.X.P. Almodovar, G. Carta, G. Ferreira, D. Robbins, Adsorption kinetics of deamidated antibody variants on macroporous and dextran-grafted cation exchangers. III. Microscopic studies, J. Chromatogr. A. 1218 (2011) 8027–8035, doi:10.1016/j.chroma.2011.09.010.
[22] E.X. Perez-Almodovar, Y. Wu, G. Carta, Multicomponent adsorption of monoclonal antibodies on macroporous and polymer grafted cation exchangers, J. Chromatogr. A. 1264 (2012) 48–56, doi:10.1016/j.chroma.2012.09.064.
[23] S.J. Traylor, X. Xu, A.M. Lenhoff, Shrinking-core modeling of binary chromatographic breakthrough, J. Chromatogr. A. 1218 (2011) 2222–2231, doi:10.1016/j.chroma.2011.02.020.
[24] A. Matlschweiger, P. Fuks, G. Carta, R. Hahn, Hindered diffusion of proteins in mixture adsorption on porous anion exchangers and impact on flow-through purification of large proteins, J. Chromatogr. A. 1585 (2019) 121–130, doi:10.1016/j.chroma.2018.11.060.
[25] E.B. Schirmer, G. Carta, Protein adsorption in charged agarose gels studied by light microscopy, AIChE J 53 (2007) 1472–1482, doi:10.1002/aic.11191.
[26] A. Ljunglöf, R. Hjorth, Confocal microscopy as a tool for studying protein adsorption to chromatographic matrices, J. Chromatogr. A. 743 (1996) 75–83, doi:10.1016/0021-9673(96)00290-7.
[27] J. Hubbuch, M.R. Kula, Confocal laser scanning microscopy as an analytical tool in chromatographic research, Bioprocess Biosyst. Eng. 31 (2008) 241–259, doi:10.1007/s00449-008-0197-5.
[28] C.A. Teske, M. Schroeder, R. Simon, J. Hubbuch, Protein-labeling effects in confocal laser scanning microscopy, J. Phys. Chem. B. 109 (2005) 13811–13817, doi:10.1021/jp050713+.
[29] C.A. Teske, E. von Lieres, M. Schröder, A. Ladiwala, S.M. Cramer, J.J. Hubbuch, Competitive adsorption of labeled and native protein in confocal laser scanning microscopy, Biotechnol. Bioeng. 95 (2006) 58–66, doi:10.1002/bit.20940.
[30] K. Yang, Q.-H. Shi, Y. Sun, Modeling and simulation of protein uptake in cation exchanger visualized by confocal laser scanning microscopy, J. Chromatogr. A. 1136 (2006) 19–28, doi:10.1016/j.chroma.2006.09.036.
[31] C.A. Teske, R. Simon, A. Niebisch, J. Hubbuch, Changes in retention behavior of fluorescently labeled proteins during ion-exchange chromatography caused by different protein surface labeling positions, Biotechnol. Bioeng. 98 (2007) 193–200, doi:10.1002/bit.21374.
[32] A. Seidel-Morgenstern, L.C. Keßler, M. Kaspereit, New developments in simulated moving bed chromatography, Chem. Eng. Technol. 31 (2008) 826–837, doi:10.1002/ceat.200800081.
[33] T. Müller-Späth, M. Krättli, L. Aumann, G. Ströhlein, M. Morbidelli, Increasing the activity of monoclonal antibody therapeutics by continuous chromatography (MCSGP), Biotechnol. Bioeng. 107 (2010) 652–662, doi:10.1002/bit.22843.
[34] R. Godawat, K. Brower, S. Jain, K. Konstantinov, F. Riske, V. Warikoo, Periodic counter-current chromatography – design and operational considerations for integrated and continuous purification of proteins, Biotechnol. J. 7 (2012) 1496–1508, doi:10.1002/biot.201200068.
[35] M. Wellhoefer, W. Sprinzl, R. Hahn, A. Jungbauer, Continuous processing of recombinant proteins: integration of refolding and purification using simulated moving bed size-exclusion chromatography with buffer recycling, J. Chromatogr. A. 1337 (2014) 48–56, doi:10.1016/j.chroma.2014.02.016.
[36] D.W. Green, R.H. Perry, Adsorption and ion exchange, in: Perrys Chem. Eng. Handb. Eighth Ed., McGraw-Hill Education, 2008: pp. 1–69.
[37] C.A. Brooks, S.M. Cramer, Steric mass-action ion exchange: displacement profiles and induced salt gradients, AIChE J 38 (1992) 1969–1978, doi:10.1002/aic.690381212.
[38] R.K. Lewus, G. Carta, Protein diffusion in charged polyacrylamide gels: visualization and analysis, J. Chromatogr. A. 865 (1999) 155–168, doi:10.1016/S0021-9673(99)00862-6.
[39] U. Altenhöner, M. Meurer, J. Strube, H. Schmidt-Traub, Parameter estimation for the simulation of liquid chromatography, J. Chromatogr. A. 769 (1997) 59–69, doi:10.1016/S0021-9673(97)00173-8.

[40] T. Kataoka, H. Yoshida, K. Ueyama, Mass transfer in laminar region between liquid and packing material surface in the packed bed, J. Chem. Eng. Jpn. 5 (1972) 132–136, doi:10.1252/jcej.5.132.
[41] E.J. Wilson, C.J. Geankoplis, Liquid mass transfer at very low reynolds numbers in packed beds, Ind. Eng. Chem. Fundam. 5 (1966) 9–14, doi:10.1021/i160017a002.
[42] S. Leweke, E. von Lieres, Chromatography analysis and design toolkit (CADET), Comput. Chem. Eng. 113 (2018) 274–294, doi:10.1016/j.compchemeng.2018.02.025.
[43] M.S. Saunders, J.B. Vierow, G. Carta, Uptake of phenylalanine and tyrosine by a strong-acid cation exchanger, AIChE J 35 (1989) 53–68, doi:10.1002/aic.690350106.
[44] M.T. Tyn, T.W. Gusek, Prediction of diffusion coefficients of proteins, Biotechnol. Bioeng. 35 (1990) 327–338, doi:10.1002/bit.260350402.
[45] H. Brenner, L.J. Gaydos, The constrained brownian movement of spherical particles in cylindrical pores of comparable radius: models of the diffusive and convective transport of solute molecules in membranes and porous media, J. Colloid Interface Sci. 58 (1977) 312–356, doi:10.1016/0021-9797(77)90147-3.
[46] G. Carta, A.R. Ubiera, T.M. Pabst, Protein mass transfer kinetics in ion exchange media: measurements and interpretations, Chem. Eng. Technol. 28 (2005) 1252–1264, doi:10.1002/ceat.200500122.
[47] Y. Tao, G. Carta, G. Ferreira, D. Robbins, Adsorption of deamidated antibody variants on macroporous and dextran-grafted cation exchangers: I. Adsorption equilibrium, J. Chromatogr. A. 1218 (2011) 1519–1529, doi:10.1016/j.chroma.2011.01.049.
[48] E.X.P. Almodóvar, Y. Tao, G. Carta, Protein adsorption and transport in cation exchangers with a rigid backbone matrix with and without polymeric surface extenders, Biotechnol. Prog. 27 (2011) 1264–1272, doi:10.1002/btpr.643.
[49] B.D. Bowes, S.J. Traylor, S.M. Timmick, K.J. Czymmek, A.M. Lenhoff, Insights into protein sorption and desorption on dextran-modified ion-exchange media, Chem. Eng. Technol. 35 (2012) 91–101, doi:10.1002/ceat.201100304.
[50] B.D. Bowes, A.M. Lenhoff, Protein adsorption and transport in dextran-modified ion-exchange media. II. Intraparticle uptake and column breakthrough, J. Chromatogr. A. 1218 (2011) 4698–4708, doi:10.1016/j.chroma.2011.05.054.
[51] B.D. Bowes, H. Koku, K.J. Czymmek, A.M. Lenhoff, Protein adsorption and transport in dextran-modified ion-exchange media. I: adsorption, J. Chromatogr. A. 1216 (2009) 7774–7784, doi:10.1016/j.chroma.2009.09.014.
[52] R. Bhambure, J.M. Angelo, C.M. Gillespie, M. Phillips, H. Graalfs, A.M. Lenhoff, Ionic strength-dependent changes in tentacular ion exchangers with variable ligand density. II. Functional properties, J. Chromatogr. A. 1506 (2017) 55–64, doi:10.1016/j.chroma.2017.05.021.
[53] S. Zhang, T. Iskra, W. Daniels, J. Salm, C. Gallo, R. Godavarti, G. Carta, Structural and performance characteristics of representative anion exchange resins used for weak partitioning chromatography, Biotechnol. Prog. 33 (2017) 425–434, doi:10.1002/btpr.2412.
[54] K. Mihlbachler, Multicolumn continuous chromatography: understanding this enabling technology, in: Contin. Biomanufacturing - Innov. Technol. Methods, John Wiley & Sons, Ltd, 2017: pp. 321–368. https://doi.org/10.1002/9783527699902.ch12.
[55] T. Müller-Späth, M. Morbidelli, Continuous Chromatography in Biomanufacturing*, in: Contin. Biomanufacturing - Innov. Technol. Methods, John Wiley & Sons, Ltd, 2017: pp. 393–422. https://doi.org/10.1002/9783527699902.ch14.
[56] D. Pfister, L. David, M. Holzer, R.-M. Nicoud, Designing affinity chromatographic processes for the capture of antibodies. Part I: a simplified approach, J. Chromatogr. A. 1494 (2017) 27–39, doi:10.1016/j.chroma.2017.02.070.
[57] D.-Q. Lin, Q.-L. Zhang, S.-J. Yao, Model-assisted approaches for continuous chromatography: current situation and challenges, J. Chromatogr. A. 1637 (2021) 461855, doi:10.1016/j.chroma.2020.461855.